A&A 581, A120 (2015)
DOI: 10.1051/0004-6361/201424048
© ESO 2015

Astronomy & Astrophysics

Hundreds of new cluster candidates in the VISTA Variables in the Vía Láctea survey DR1⋆

R. H. Barbá[1], A. Roman-Lopes[1], J. L. Nilo Castellón[1], V. Firpo[1], D. Minniti[2,3,4,5,6], P. Lucas[7], J. P. Emerson[8], M. Hempel[2,6], M. Soto[1,9], and R. K. Saito[10]

[1] Departamento de Física y Astronomía, Universidad de la Serena, Av. Juan Cisternas 1200 Norte, La Serena, Chile
e-mail: rbarba@userena.cl
[2] Departamento de Ciencias Físicas, Universidad Andres Bello, 220 República, Santiago, Chile
[3] Vatican Observatory, 00120 Vatican City State, Italy
[4] European Southern Observatory, 3107 Vitacura, Santiago, Chile
[5] Department of Astrophysical Sciences, Princeton University, Princeton, NJ 08544-1001, USA
[6] The Milky Way Millennium Nucleus, Av. Vicuña Mackenna 4860, 782-0436 Macul, Santiago, Chile
[7] Centre for Astrophysics Research, Science and Technology Research Institute, University of Hertfordshire, Hatfield AL10 9AB, UK
[8] Astronomy Unit, School of Physics and Astronomy, Queen Mary University of London, Mile End Road, London, E1 4NS, UK
[9] Space Telescope Science Institute, MD 21117, USA
[10] Universidade Federal de Sergipe, Departamento de Física, Av. Marechal Rondon s/n, 49100-000 São Cristóvão, SE, Brazil

Received 22 April 2014 / Accepted 12 January 2015

ABSTRACT

Context. VISTA variables in the Vía Láctea is an ESO Public survey dedicated to scanning the bulge and an adjacent portion of the Galactic disk in the fourth quadrant using the VISTA telescope and its near-infrared camera VIRCAM. One of the leading goals of the VVV survey is to contribute to knowledge of the star cluster population of the Milky Way.
Aims. To improve the census of Galactic star clusters, we performed a systematic and careful scan of the JHK_s images of the Galactic plane section of the VVV survey.
Methods. Our detection procedure is based on a combination of stellar density maps and visual inspection of promising features in the J-, H-, and K_S-band images. The material examined are VVV JHK_S color-composite images corresponding to Data Release 1 of VVV.
Results. We report the discovery of 493 new infrared star cluster candidates. The analysis of the spatial distribution show that the clusters are very concentrated in the Galactic plane, presenting some local maxima around the position of large star-forming complexes, such as G305, RCW 95, and RCW 106. The vast majority of the new star cluster candidates are quite compact and generally surrounded by bright and/or dark nebulosities. IRAS point sources are associated with 59% of the sample, while 88% are associated with MSX point sources. GLIMPSE 8 μm images of the cluster candidates show a variety of morphologies, with 292 clusters dominated by knotty sources, while 361 clusters show some kind of nebulosity in this wavelength regime. Spatial cross-correlation with young stellar objects, masers, and extended green-object catalogs suggest that a large sample of the new cluster candidates are extremely young. In particular, 104 star clusters associated with methanol masers are excellent candidates for ongoing massive star formation. Also, there is a special set of sixteen cluster candidates that present clear signposts of star-forming activity having associated simultaneosly dark nebulae, young stellar objects, extended green objects, and masers.

Key words. open clusters and associations: general – Galaxy: stellar content – Galaxy: structure – infrared: stars – surveys

1. Introduction

Stellar clusters play a fundamental role in the dynamics and chemical evolution of galaxies. They trace recent star formation history and display some of the most spectacular scenarios of stellar evolution. Indeed, knowing how the clustered stellar populations are distributed within our galaxy is essential in the study of its large scale structure, hence a key objective of large surveys like VISTA Variables in the Vía Láctea (VVV, Minniti et al. 2010). However, newborn stars formed in clustered environments are often embedded in large or giant molecular clouds that generate heavy obscuration, which hinder optical observations of their early development stages, so observations at infrared wavelengths are preferred (Lada & Lada 2003).

In the particular case of the Milky Way, any study of its global structure and morphology is difficult because we are looking at it from a location whitin the Galactic plane, where the bulk of the gas, dust, and stars are known to be confined, making the extinction and crowding extremely complex and high. Because of that, and in spite of developments in instrumentation and observational techniques, a significant fraction of the Milky Way cluster population remains unknown. In fact, it has been estimated that our galaxy should have at least ~23 000[1] open clusters (Portegies Zwart et al. 2010), however only a few thousand of them have been identified to date.

⋆ Full Tables 1–3 are only available at the CDS via anonymous ftp to cdsarc.u-strasbg.fr (130.79.128.5) or via http://cdsarc.u-strasbg.fr/viz-bin/qcat?J/A+A/581/A120

[1] This number is a lower limit for the estimated population of star clusters in the Galaxy. Bonatto et al. (2006) indicated a total number of open clusters in the range $1.8–3.7 \times 10^5$.

Customarily, the detections of new Galactic star clusters are mostly based on a visual inspection of recorded photographic and electronic images (CCDs, IR detectors, etc.) taken both at optical and near-infrared wavelengths, and the development of new homogeneous surveys in the past decade has allowed the discovery and analysis of many previously unknown cluster candidates: e.g., Bica et al. (2003), Dutra et al. (2003), Mercer et al. (2005), Froebrich et al. (2007), Borissova et al. (2011), Solin et al. (2014), etc. Particularly relevant to our research is the Two-Micron All-Sky Survey (2MASS, Skrutskie et al. 2006), the prior near-infrared all sky survey, covering the same wavelength range as VVV, but with different spatial resolution (4.″0 vs. 0.″7) and photometric depth (K_S-mag 15.5 vs. 18 in VVV). Also, if we consider that open clusters are gravitationally bound structures that consist of more or less coeval stellar populations, the detection of density enhancements, either visually or by means of computational algorithms, should be only the first step to properly identifying potential new clusters. Indeed, stellar density enhancements may also be produced by chance alignments or localized low foreground extinction (e.g., Odenkirchen & Soubiran 2002; Maciejewski & Niedzielski 2008; Moni Bidin et al. 2010; Froebrich et al. 2007). In this sense, to confirm that a group of stars are really physically related and forming a true cluster, some additional criteria such as radial density profiles (e.g., Gaussian or King), colors, and/or kinematics, are probably necessary. Besides that, the HIPPARCOS catalog (ESA 1997) has provided accurate positions (as probably *Gaia* will do in the future), proper motions, and trigonometric parallaxes for a significant stellar population in the solar neighborhood. For example, many OB associations show small velocity dispersions (e.g., Tian et al. 1996), which makes them appear as coherent structures in velocity space, and de Zeeuw et al. (1999) used this characteristic to distinguish the membership in the HIPPARCOS catalog of nearby OB associations inside a ∼1 kpc radius of the solar neighborhood.

Here we present the results of our search for new cluster candidates in the Galactic disk portion covered by the VVV Data Release 1 (DR1) images (Saito et al. 2012). This work is based on stellar density maps and visual inspection of the associated J-, H-, and K_S-band VVV DR1 images. As a result almost 500 new Galactic cluster candidates were identified in the disk area of the VVV survey. To make this catalog, we performed a more systematic search in each VVV tile than Borissova et al. (2011) using the same set of VVV DR1 images. This paper is organized as follow: in Sect. 2, we describe briefly the main characteristics of the VVV. In Sect. 3, we describe the finding methods for the new star cluster candidates. In Sect. 4, we describe the characteristics of the new star clusters and the spatial cross-correlation with different infrared and radio source catalogs, and in the Sect. 5, we summarize our conclusions.

2. Data: VVV tile images

The VVV survey observations are being carried out in the four-meter Visible and Infrared Survey Telescope for Astronomy (VISTA), using the VIRCAM (VISTA InfraRed CAMera; Dalton et al. 2006; Emerson & Sutherland 2010) located at ESO's Cerro Paranal Observatory in Chile. VIRCAM has a field of view of 1.65° diameter, but the sparse mosaic of 4 × 4 Raytheon 2048 × 2048 pixels^2 detectors (spacing of 40% and 90% in the X and Y axes, respectively), only covers 0.6 deg^2 in each single pointing (a *pawprint*), with a pixel scale of 0.″34. Six suitably offset VISTA pawprints are combined to form a contiguous 1.5 × 1.0 deg^2 area known as a *tile*, which covers each piece of the sky at least twice, except for single exposures at the upper and lower extremes in Y. The VVV survey was planned to observe 348 of these fields in the Galactic bulge and a portion of the Southern Galactic disk (196 and 152 tiles, respectively), in five broadband filters Z, Y, J, H, K_S. The area covered by the VVV survey overlaps completely with the 2MASS survey, with part of the *Spitzer* Space Telescope GLIMPSE survey (Benjamin et al. 2003), and also complements the area covered by the UKIDSS survey (Lucas et al. 2008).

This work is based on the analysis of the 152 J, H, and K_S Galactic plane tile images, which were produced by the Cambridge Astronomical Survey Unit (CASU) from the scheduled observations of the first and second years of the survey. These images are available as DR1 (Saito et al. 2012). Further details about the VVV survey, technical description, observing strategy, and scientific goals are in Minniti et al. (2010).

3. Star cluster candidate finding methods

Our approach for detecting and selecting each new star cluster candidate was to look for variations in the stellar density by simple star counts, helped by the systematic examination of the tile image of each band and the combined color mosaics displayed in the Aladin virtual observatory tool (Bonnarel et al. 2000). The selected color combination was the usual: J, H, and K_S images combined as blue, green, and red channels, respectively. The star-count methodology is well known and has been used by several researchers (e.g., Lada & Lada 1995; Carpenter et al. 1995, 2000; Kumar et al. 2004, 2006). The method can be refined by using different bin sizes in order to investigate large-scale structures, as well as smaller scale subclustering (e.g., Kumar et al. 2004; Kirsanova et al. 2008), and/or also by smoothing the binned data over adjacent bins (e.g., Karampelas et al. 2009).

The star-count technique was applied to the Galactic disk portion of the VVV DR1 K_S-band images. The stars were detected using the task DAOFIND (Package DAOPHOT) in IRAF[2]. The limiting magnitudes are those for point sources presenting minimum peak count values, of 3σ above the local sky, which in general correspond to J, H, and K_S magnitude values of about 19.5, 18.8, and 18, respectively. Of course, such values must be considered as mean values because the numbers depend critically on the position of the sources relative to zones of extended emission, as well as to the heavily crowded zones like those in the Galactic plane. The technique consists of dividing each tile into small bins of equal size and determining the number of stars in each bin. As result, those bins presenting values greater than 3σ above what was measured in a given control region were considered as locations of potential candidate clusters, deserving further examination "by eye". The binning sizes were chosen carefully such that the number of objects per bin was neither too small (prohibiting a meaningful analysis) nor too large (hiding existing features).

We used tipical bin sizes varying from 30 pixels (about 10″) to about 90 pixels (about 30″), which were determined empirically on known cluster candidates in the H II regions RCW 106 and RCW 95, which were previously studied in the past by one of us (ARL).

As a quantitative example of the procedure applied in the detection of a local maximum in the stellar density maps on

[2] IRAF is distributed by the National Optical Astronomy Observatories, which are operated by the Association of Universities for Research in Astronomy, Inc., under cooperative agreement with the National Science Foundation.

the K_S-band VVV images, for a "small" cluster candidate like La Serena 004 (with an estimated radius smaller than 30″), the binning size that enabled us to detect it with a appropriate contrast against the surrounding field stars was 5″. On the other hand, for a "large" cluster candidate like La Serena 012, the best results were achieved when we applied the biggest binning size of 30″. Of course, we must point out that using this binning range possibly led to a cluster candidate detection rate biased toward small-to-medium sized cluster candidates, with most of the larger and sparse clusters being hard to detect. The control regions used in determining of the mean background to be subtracted from the statistics for each cluster candidate were computed from concentric rings with a mean radius equivalent to two to three times the observed estimated size of the respective cluster candidate. We also tested the use of adjacent control fields placed at several arc minutes (typically 2−5) from the center of the cluster candidate, finding no significant differences between each method.

Finally, stellar density maps were then compared with the color-composite JHK_S images, which in turn were used to properly evaluate and identify (by visual inspection of the local concentrations of stars) those features related to candidate clusters. The presence of artefacts around saturated stars have artificially increased the star counts around many cluster candidates. We must take into account that in the VVV images, the saturation limit in the K_S-band images is about magnitude 12.5. Additionally, we visually identified some compact stellar groups mostly associated with bright and/or dark nebulosities. If such a close association was confirmed, the cluster candidate was evaluated for overdensities and included in the catalog. Also, during the search, we discovered some concentrations of saturated bright sources in the VVV images, but their appearance resembles a cluster of red giant or supergiant stars, similar in morphology to some clusters discovered in the 2MASS survey (cf. Figer et al. 2006; Clark et al. 2009). We included some of these groups after considering the 2MASS data for the saturated stars, for example, the star cluster candidate labeled as La Serena 109. We checked carefully that each stellar group candidate had been not discovered previously, and any previously known neighbor cluster should be located at the minimum distance of one arcminute.

Catalogs of star clusters and star cluster candidates used for the check are Bica et al. (2003), Dutra et al. (2003), Mercer et al. (2005), Froebrich et al. (2007), and Borissova et al. (2011). Recently, Solin et al. (2014) have published a new catalog with star cluster candidates, using the same set of Galactic disk VVV DR1 images and also including the bulge area. These authors report 88 new star cluster candidates and 39 star formation location candidates detected by a fit of a mixture model of Gaussian densities and background noise, and the expectation maximization algorithm to prefiltered near-infrared survey stellar catalog data.

Interestingly, this independent search of cluster candidates is a very good check on the reliability of our methods. In the VVV tiles of the Galactic disk, Solin et al. (2014) detect 82 star cluster candidates, 34 star formation location candidates, and 24 infrared nebulae of unknown nature. We performed a cross-match with a radius of 60″ between our catalog and Solin et al. (2014) sources, obtaining a very good agreement. We "recover" 111 sources from the complete list of 140 objects in the Solin et al. (2014), which are 105 sources inside the 15″ cross-matching radius. The "recovered" objects from the Solin et al. (2014) correspond to 68 cluster candidates (83% of Solin et al. list), 25 star forming region candidates (73%), and 18 infrared nebulae (75%).

In Table 1 we present a sample of the catalog, as an example of its form and content. The full catalog includes 493 star cluster candidates, and it is hosted by CDS database and also the VVV-ULS[3] project page. Characteristics listed in Cols. 7 to 11 will be described in the following sections. The catalog is organized as follows:

Column 1: lists the star cluster candidate designation La Serena and running numbers from 1 to 493.
Columns 2 to 5: gives the equatorial (J2000.0 epoch) and galactic coordinates of the cluster center. These coordinates are estimated from the bin center, and in many cases they are corrected with inspection of the images by eye.
Column 6: indicates the VVV tile where the cluster is located. In a few cases, when the cluster is close to the edge of the tile, it is possible to find it in two different tiles.
Column 7: lists the IRAS source associated with the cluster.
Column 8: lists the MSX source associated with the cluster.
Column 9: indicates the morphological appearance of the cluster: O (open cluster) or C (compact cluster). Compact clusters are small clumps of stars, with sizes less than 30″, mostly associated with compact nebulosities in the VVV and/or GLIMPSE 8 μm images, while on the other hand, larger extended clusters are classified as open clusters.
Column 10: describes the size of the clusters based on an upper-limit estimation of the number of sources (N_s) associated with the cluster. Star clusters with $N_s < 20$ are classified as small (S). Those with $20 < N_s < 50$ are classified as medium (M). Finally, clusters with $N_s > 50$ are classified as large (L). We estimate these upper limits from the star count in the area of the cluster, doing an eyeball estimation of the size of the cluster. These numbers are for guidance because it must be noted that no background or crowding correction were applied.
Column 11: describes the morphology of each cluster based on 8 μm band images obtained by the *Spitzer* Space Telescope, under GLIMPSE survey. There are four main morphological types: point sources (P), knots (K), bubbles (B or sB), and nebula (N). Additional comments about the morphology of the clusters are noted in Table 2. Point sources refer directly to a group of point sources without noticeable nebulosity. Knot refers to a remarkable and compact nebulosity associated with point sources in the 8 μm images. Bubble refers to arc-shaped nebulosity associated with the point sources. In some cases the arcs or filaments form small circles delimiting small cavities in the dusty clouds, while in other cases, the arcs define larger bubbles. For the case of small bubbles, they are marked as sB. Nebula refers to diffuse nebula without a specific shape associated with the point sources.

Also, we present in Table 2 a sample of the association of different astrophysical sources with each cluster candidate obtained in the cross-matching procedures described in Sect. 4.2. Again the full table is available in the CDS database. Table 2 lists the Solin et al. (2014) object name (Col. 2) and the different types of objects associated with the new star cluster candidates: dark clouds (Col. 3), young stellar object candidates (Col. 4), extended green objects and outflows (Col. 5), and masers, with the corresponding bibliographic references (Cols. 6 and 7).

Additionally, in Table 3 special notes and comments for each cluster candidate are included.

We have prepared a website with the detailed astrometric and morphologic information for the 493 cluster candidates,

[3] http://astro.userena.cl/science/lsclusters.php

Table 1. La Serena star cluster candidates.

Cluster ID	RA_{J2000}	Dec_{J2000}	ℓ	b	Tile	IRAS source	MSX source	Type	Size	8 μm morphology
La Serena 001	11:39:13	−63:29:04	294.9726	−1.7292	d001	IRAS 11368-6312	G294.9725-01.7290	C	M	–
La Serena 002	11:39:22	−63:28:11	294.9896	−1.7188	d001	–	G294.9895-01.7186	C	M	–
La Serena 003	11:40:28	−63:27:58	295.1026	−1.6779	d001	IRAS 11380-6311	G295.1026-01.6778	C	S	–
La Serena 004	11:42:09	−62:20:07	294.9846	−0.5365	d039	–	G294.9845-00.5363	O	M	P+N
La Serena 005	11:43:25	−62:25:43	295.1523	−0.5891	d039	–	G295.1523-00.5890	O	S	–
La Serena 006	11:43:28	−62:27:20	295.1652	−0.6072	d039	–	G295.1651-00.6070	O	L	P
La Serena 007	11:43:38	−62:25:17	295.1750	−0.5738	d039	IRAS 11412-6208	G295.1750-00.5737	O	L	K+N
La Serena 008	11:44:34	−62:40:47	295.3450	−0.7950	d039	IRAS 11421-6223	G295.3450-00.7949	O	S	sB
La Serena 009	11:45:04	−63:17:44	295.5571	−1.3788	d001	IRAS 11426-6301	G295.5570-01.3787	C	M	–
La Serena 010	11:47:05	−62:38:31	295.6194	−0.6887	d039	–	G295.6194-00.6886	O	M	P
La Serena 011	11:50:13	−62:08:44	295.8504	−0.1183	d039	IRAS 11478-6152	G295.8503-00.1182	O	M	P+K
La Serena 012	11:50:25	−62:49:13	296.0283	−0.7693	d039	–	–	O	M	P
La Serena 013	11:53:12	−62:30:18	296.2654	−0.3903	d040	IRAS 11507-6213	G296.2654-00.3901	O	M	P+K
La Serena 014	11:54:15	−62:51:41	296.4640	−0.7096	d040	IRAS 11517-6234	G296.4640-00.7094	C	M	K
La Serena 015	11:55:23	−63:25:30	296.7131	−1.2336	d002	IRAS 11528-6308	G296.7130-01.2335	C	S	–
La Serena 016	11:55:53	−62:54:35	296.0283	−0.7693	d040	–	–	O	S	P
La Serena 017	12:00:57	−63:04:04	297.2535	−0.7558	d040	IRAS 11583-6247	G297.2535-00.7557	O	S	K+sB
La Serena 018	12:02:21	−62:36:32	297.3249	−0.2679	d040	IRAS 11597-6220	G297.3249-00.2678	O	L	P+N
La Serena 019	12:02:45	−63:07:02	297.4585	−0.7637	d040	–	G297.4585-00.7636	O	S	K+N
La Serena 020	12:03:16	−63:11:15	297.5343	−0.8266	d040	–	G297.5343-00.8264	O	L	K
La Serena 021	12:03:54	−62:22:34	297.4538	−0.0094	d040	IRAS 12013-6205	G297.4537-00.0093	C	M	K+P
La Serena 022	12:03:57	−63:17:08	297.6252	−0.9044	d040	IRAS 12013-6300	G297.6252-00.9043	C	M	K+N
La Serena 023	12:12:20	−64:15:18	298.6992	−1.7068	d003	IRAS 12096-6358	G298.6992-01.7067	O	M	–
La Serena 024	12:12:29	−62:49:49	298.5028	−0.2900	d041	–	G298.5028-00.2899	O	L	P+N
La Serena 025	12:12:53	−62:44:46	298.5355	−0.2051	d041	–	G298.5354-00.2049	O	L	P
La Serena 026	12:12:58	−61:50:25	298.4088	+0.6938	d079	IRAS 12102-6133	G298.4087+00.6938	O	M	P+N
La Serena 027	12:15:57	−62:28:00	298.8450	+0.1221	d079	IRAS 12132-6211	G298.8449+00.1221	O	M	K+N
La Serena 028	12:16:43	−62:14:26	298.8878	+0.3599	d079	IRAS 12140-6157	G298.8877+00.3599	O	M	K+P
La Serena 029	12:18:28	−62:37:17	299.1532	+0.0086	d042	IRAS 12157-6220	G299.1531+00.0086	C	M	K
La Serena 030	12:19:38	−62:57:21	299.3244	−0.3068	d042	IRAS 12169-6240	G299.3244-00.3067	O	L	K+B
La Serena 031	12:19:54	−62:55:42	299.3547	−0.2750	d042	IRAS 12171-6238	G299.3546-00.2749	O	M	K+N
La Serena 032	12:23:08	−62:40:50	299.6907	+0.0009	d080	–	G299.6906+00.0010	O	M	P+B
La Serena 033	12:23:48	−62:42:28	299.7701	−0.0061	d080	IRAS 12210-6225	G299.7700-00.0060	C	M	K
La Serena 034	12:28:42	−63:26:19	300.3932	−0.6790	d042	IRAS 12259-6309	–	O	M	P
La Serena 035	12:28:51	−63:02:40	300.3770	−0.2858	d042	–	G300.3770-00.2857	C	M	K+P
La Serena 036	12:32:22	−62:41:20	300.7487	+0.1016	d081	IRAS 12295-6224	G300.7486+00.1016	O	M	K+sB
La Serena 037	12:34:17	−61:55:17	300.9121	+0.8830	d081	IRAS 12314-6138	G300.9121+00.8830	O	M	K

Notes. Only a small portion of the data is provided here, the full table is only available in electronic form at the CDS.

Table 2. Association with different astrophysical sources.

Cluster Id	Solin et al. (2014)	Dark nebulae	YSO candidates	EGO and outflows	Masers	Maser references
La Serena 001					CH3OH [VES2000] 113651.54-631209.4	2000MNRAS.317..315V
					H2O [BSG89] 294.97-1.73	1989A&AS...77..465B
La Serena 002					CH3OH MMB 294.990-1.719	2012MNRAS.420.3108G
La Serena 003	G295.103-1.677					
La Serena 004	G294.988-0.539					
La Serena 005		SDC G295.137-0.594	SSTGLMC G295.1417-00.5891			
		SDC G295.136-0.563				
La Serena 006		SDC G295.137-0.594				
La Serena 007	G295.176-0.574	SDC G295.185-0.578				
La Serena 008		SDC G295.353-0.809				
		SDC G295.362-0.787				
La Serena 009	G295.557-1.378		[MHL2007] G295.5570-01.3787 1			
La Serena 010						
La Serena 011		SDC G295.860-0.139				
La Serena 012						
La Serena 013			[MHL2007] G296.2654-00.3901 1			
La Serena 014						
La Serena 015						
La Serena 016						
La Serena 017	G297.253-0.754	SDC G297.275-0.741	SSTGLMC G297.2615-00.7433			
		SDC G297.268-0.776				
La Serena 018		SDC G297.313-0.294				
La Serena 019		SDC G297.440-0.762				
La Serena 020	G297.533-0.823	SDC G297.523-0.814				
		SDC G297.539-0.842				
La Serena 021		SDC G297.451+0.002				
La Serena 022						
La Serena 023			[MHL2007] G298.6992-01.7067 1			
La Serena 024		SDC G298.479-0.314	SSTGLMC G298.5010-00.2878			
La Serena 025		SDC G298.519-0.212				
La Serena 026			SSTGLMC G298.4047+00.6998			
La Serena 027		SDC G298.858+0.151		EGO G298.90+0.36		
				EGO G298.89+0.37		
La Serena 028	G298.903+0.358	SDC G298.904+0.354	SSTGLMC G298.9063+00.3548			
		SDC G298.901+0.349	SSTGLMC G298.8877+00.3596			
La Serena 029		SDC G299.167+0.010				
La Serena 030	G299.325-0.308	SDC G299.333-0.294				
		SDC G299.302-0.305				
		SDC G299.350-0.324				
La Serena 031		SDC G299.349-0.252				
La Serena 032						
La Serena 033					CH3OH MMB 299.772-0.005	2012MNRAS.420.3108G
La Serena 034						
La Serena 035			SSTGLMC G300.3797-00.2862			
La Serena 036		SDC G300.743+0.128				
La Serena 037		DOBASHI 5897	SSTGLMC G300.9071+00.8828			

Notes. Only a small portion of the data is provided here, the full table is only available in electronic form at the CDS.

Table 3. Special notes and comments for each cluster candidate.

Cluster ID	Notes
La Serena 001	1.6′ from cluster VVV-CL 005. 1.8′ from IC 2944 and 1′ from IC 2948
La Serena 002	1.4′ from cluster VVV-CL 101
La Serena 003	4′ from IC 2944
La Serena 004	
La Serena 005	In HII region [WMG70] 295.2-00.6
La Serena 006	Projected on open cluster Stock 14
La Serena 007	5′ from open cluster Stock 14, and 1.3′ from SNR G295.2-00.6
La Serena 008	
La Serena 009	
La Serena 010	Identified also as cluster FSR 1595
La Serena 011	
La Serena 012	
La Serena 013	
La Serena 014	
La Serena 015	
La Serena 016	
La Serena 017	
La Serena 018	
La Serena 019	HII region GAL 297.51-00.77, 3′ from cluster Mercer 29, in the edge of bubble
La Serena 020	3.5′ from cluster Mercer 29
La Serena 021	
La Serena 022	In molecular cloud [RC2004] G297.6-0.9+30.3
La Serena 023	
La Serena 024	In the edge of large bubble, cluster Mercer 30 inside.
La Serena 025	2.6′ from cluster DSH J1213.0-6242
La Serena 026	HII region. It is not PN G298.4+00.6. Reflection nebula GN 12.10.3
La Serena 027	
La Serena 028	
La Serena 029	Dark nebula SDC G299.167+0.010
La Serena 030	Reflection nebula BRAN 386C, in the wall of bubble [CPA2006] S175. Part of RCW 64.
La Serena 031	3.4′ from cluster VVV-CL 012. Part of RCW 64. HII region BRAN 386E
La Serena 032	In the center of bubble [CPA2006] S174
La Serena 033	In the edge of bubble [CPA2006] S174, 4.8′ from cluster VVV-CL 032
La Serena 034	
La Serena 035	
La Serena 036	
La Serena 037	

Notes. Only a small portion of the data is provided here, the full table is only available in electronic form at the CDS.

including color-composite charts. This catalog is available at the VVV-ULS project page. These color-composite images were created by combining J-band, H-band, and K_S-band images following the usual scheme of blue, green, and red channels. Each color image was cropped and dynamically stretched to display each cluster comfortably. For example, the chart for the compact cluster La Serena 309 was cropped to a size of $1' \times 1'$, while the chart corresponding to the open cluster candidate La Serena 109 was cropped to a $3' \times 3'$ field of view, respectively. As example, Fig. 1 presents JHK_S color-composite images of some of the newly discovered star cluster candidates. The complete set of color-composite chart images will be available in VVV-ULS web page.

4. Characteristics of the new cluster candidates

4.1. Spatial distribution

The angular distribution of the new stellar group candidates (Fig. 2, upper left panel) shows an obvious concentration toward the Galactic plane. The distribution in Galactic latitude is characterized by a single-peaked distribution with a half-width at half-maximun of about 0.6° (Fig. 2, upper right panel). The peak of distribution is slightly shifted −0.2° from the Galactic plane. The distribution in Galactic longitude shows the presence of many groups of clusters associated with large star-forming complexes (Fig. 2, lower panel). For example, clusters located at $l = 305° - 306°$ are associated with the star-forming complex G305; at $l = 309°$ are associated with the H II region RCW 80, clusters located at $l = 310°$ with the H II region RCW 83, at $l = 326°$ with the star-forming complex RCW 95 and RCW 97, at $l = 333°-334°$ with the star-forming complex RCW 106, at $l = 339°$ with H II region RCW 109, and the small maximum of cluster count located at $l = 346°$ with the giant molecular complex GMC 345.5+1.0 (López et al. 2011). We notice a decrease in the number of candidate clusters discovered at $l > 340°$, which may be related to an increase in extinction and/or increased crowding toward the inner disk, which dilutes the ability to detect poor star clusters.

4.2. Spatial correlation with other infrared sources and structures

The methodology used to detect candidates certainly favors the discovery of compact groups. Detected densities were boosted in regions near or in the dark clouds, where the number of field

Fig. 1. RGB color images of a representative sample of the newly discovered cluster candidates. The field-of-view for the chart of each cluster is set variously between 1×1 arcmin, 3×3 arcmin, and 5×5 arcmin in order to visualize the cluster comfortably. This set of clusters are the same shown in Fig. 9. The complete set of charts for the whole catalog is offered on the catalog website, see details in Sect. 3.

stars drops owing to the presence of these clouds. Most of these cluster candidates are compact groups whose stars undergo high reddening, and many times they have associated small emission nebulosities. Some examples of this kind of cluster are La Serena 045, La Serena 185, and La Serena 328. At first glance, the morphology of these star cluster candidates suggests that they are in the stage of ongoing star formation. Therefore, if the star formation processes are in such early stages, then many of these clusters could be associated with mid-infrared sources.

Therefore we performed a number of cross-matching procedures between our catalog and the different catalogs available in SIMBAD and VizieR in order to identify the mid-infrared source counterparts. The cross-matching procedures utilize the TopCat virtual observatory tool (Taylor 2005).

The first two cross-matching procedures are based on the Infrared Astronomical Satellite (IRAS) point source catalog (PSC; Beichman et al. 1988) and the Midcourse Space Experiment (MSX) catalog version 6 (MSX6C;

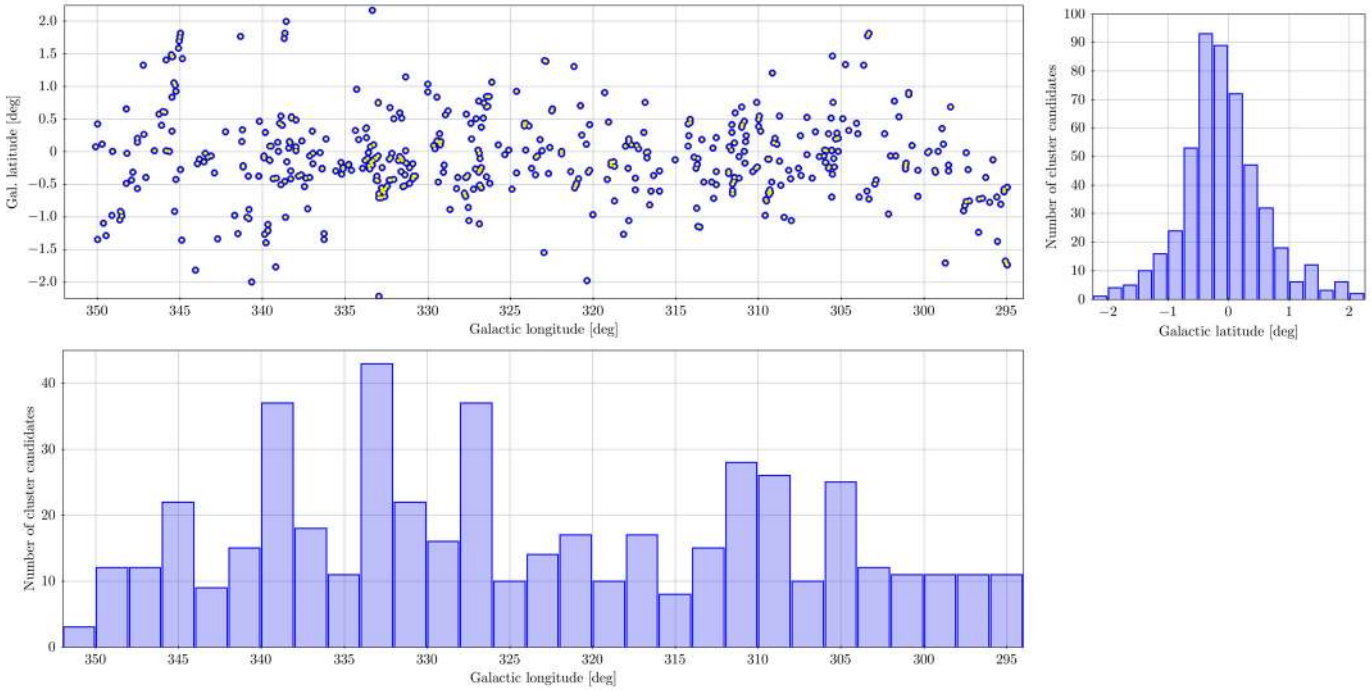

Fig. 2. Angular distribution of the newly discovered VVV-La Serena star cluster candidates in the Galactic plane (*upper left panel*). Also, the histograms of the distributions of clusters in Galactic latitude (*upper right panel*) and Galactic longitude (*lower panel*).

Egan et al. 2003). IRAS PSC includes about 250 000 reliable infrared point sources observed by the Infrared Astronomical Satellite. These sources have angular extents less than approximately 0.5, 0.5, 1.0, and 2.0 arcmin in the in-scan direction at 12, 25, 60, and 100 μm, respectively. Away from confused regions of the sky, the survey is complete to about 0.4, 0.5, 0.6, and 1.0 Jy at these wavelengths. The representative position uncertainties are about 2″ to 6″ in-scan and about 8″ to 16″ cross-scan directions, respectively. The MSX6C in the Galactic plane includes about 430 000 point sources observed with the infrared instrument SPIRIT III on MSX, with an astrometric accuracy better than 1″. This instrument consists of a 33 cm clear-aperture off-axis telescope with five line scanned infrared focal plane arrays of 18.3″ square pixels, and a high sensitivity (0.1 Jy at 8.3 μm). SPIRIT III is provided with six photometric bands: B1 (4.29 μm), B2 (4.35 μm), A (8.28 μm), C (12.13 μm), D (14.65 μm), and E (21.34 μm).

We find 293 IRAS sources closer than a cross-matching radius of 30″ (Fig. 3), corresponding to 59% of VVV cluster candidates. The matching radius used corresponds to the IRAS spatial resolution at 12 μm; however, this may be too restrictive with respect to the IRAS resolution, but will reduce the confusion with neighboring mid-infrared structures. The IRAS point sources associated with each star cluster candidate are listed in Col. 7 of Table 1.

We also matched the cluster candidates with Midcourse Space Experiment (MSX) catalog version 6 (Egan et al. 2003). Compared with IRAS, the MSX survey has better spatial resolution (18″) and sensitivity on the Galactic plane, and we might expect a tighter cross-matching. Figure 4 shows the distribution of separations for the MSX sources, using a matching radius of 30″. We have 436 MSX point sources (88%) associated with our star cluster candidates, with 50% of them inside the 8″ circle. The MSX sources associated with our source catalog are indicated in Col. 8 of Table 1. For sparse open clusters candidates, composed presumably of red giant or supergiant stars

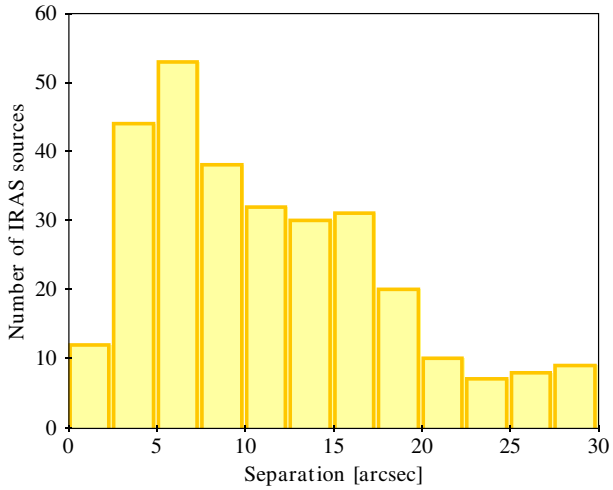

Fig. 3. Histogram of the number of IRAS point sources associated with VVV–La Serena star cluster candidates.

distributed over several square arcminutes (e.g., La Serena 314), the MSX point source listed in Table 1 corresponds to the closer source to the position derived for the cluster center.

As mentioned above, the vast majority of cluster candidates were detected in areas with dark and/or bright nebulosities on the VVV images. A visual inspection of VVV images finds a total of 456 cluster candidates associated with dark clouds up to a distance of 2′. We searched for dark cloud catalogs in the VizieR database in the area covered by the Galactic disk VVV tiles, and we find four main entries: Peretto & Fuller (2009), Dobashi (2011), Dutra & Bica (2002), and Hartley et al. (1986). The first one is the most important for our study by far. The cross-matching between our catalog and these dark cloud catalogs finds 310 cluster candidates (63%) associated with 552 dark clouds. Column 3 in Table 2 lists the dark clouds associated

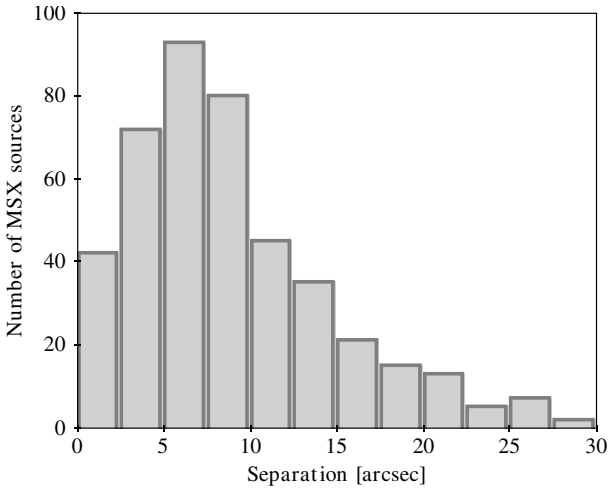

Fig. 4. Histogram of the number of MSX sources associated with VVV–La Serena star cluster candidates.

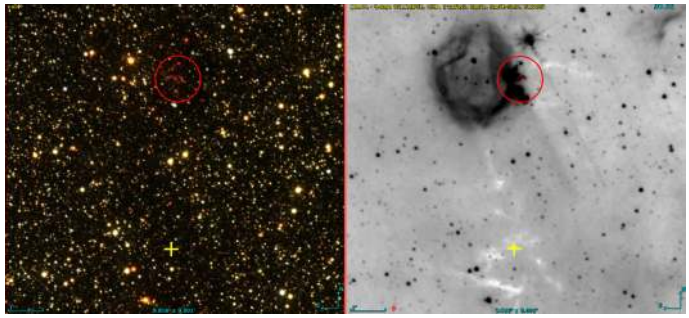

Fig. 5. Area of cluster candidate La Serena 208. *Left panel*: VVV color-composite image following the same scheme as in Fig. 1. *Right panel*: *Spitzer*/GLIMPSE 8 μm. The cluster candidate is marked with a small red circle, and the dark cloud SDC G321.336−0.373 wth a small yellow plus sign. The field of view of each panel is about 9.8 × 9.0 arcmin.

with each cluster candidate in detail. Interestingly, most of the dark nebulae change their appearance and morphology with the wavelength range of the observations. As an example, we describe the area surrounding the cluster La Serena 208. Figure 5 shows the VVV color-composite image and *Spitzer*/GLIMPSE 8 μm around this cluster. In the VVV color-composite image, it is possible to discern a filamentary dark nebula that causes a marked reddening and a decline in the star count. In the *Spitzer*/GLIMPSE 8 μm image at the position of VVV-La Serena 208 reveals a cluster of knot point sources associated with filamentary arcs that lie eastward, forming a small bubble of 1.′3 diameter, cataloged as [CPA2006] S89 (Churchwell et al. 2006). Additionally, an infrared dark cloud connected with the bubble is located 4.′8 to the south. This infrared dark cloud (IRDC), known as SDC G321.336-0.373 (Peretto & Fuller 2009), has an angular size of 0.′525 × 0.′222. Examination of the GLIMPSE 8 μm image suggests a connection between the IRDC and the bubble through a series of uncataloged dark filaments.

In view of the importance of the rich morphological information that stands out in the *Spitzer* 8 μm images, we visually inspected the nebular structures in the GLIMPSE images at the positions of the star cluster candidates, which are described in Col. 11 of Table 1 The GLIMPSE survey extends approximately from Galactic latitude −1.°2 to 1.°2, and only 441 cluster candidates are projected in that area, with all of them detectable in some way (as point sources or extended structures) in the 8 μm images. *Spitzer* 8 μm point sources are the main feature for 80 cluster candidates. Very compact nebulosity associated with point sources is present in 292 cluster candidates at that wavelength range. These kinds of sources are described as a knot. In many cases (156), these point sources and/or knots are also associated with extended irregular nebulosities (marked as nebula), and there are 89 clusters where this nebulosity is bubble-shaped, which were identified as bubbles or small bubbles. Taking the three different nebular emission structures cataloged into account, we count 361 cluster candidates with some kind of nebular emission associated at 8 μm, that means 82% of the sample in the area of GLIMPSE images. Figure 9 depicts some examples of clusters candidates as seen in GLIMPSE 8 μm images. The square plotted inside each image corresponds to the size of the VVV image charts shown in Fig. 1.

The presence of knots and nebulosities in the *Spitzer* images suggests that the clusters could be extremely young. Taking this possibility into account, we explore the spatial correlation between the cluster candidates and other independent tracers of ongoing star formation, such as masers, young stellar objects (YSO), extended green objects (EGO), and outflows.

Astrophysical maser emissions are proven signatures of ongoing star formation, in particular methanol masers (cf. Ellingsen 2006; Breen et al. 2013), although we must consider that water or hydroxyl masers have also been detected in in star-forming regions, as well as in evolved stars or supernova remnants. Therefore, the presence of these maser types in the vicinity of a cluster could be an excellent signspot that this cluster has ongoing star formation. We checked the presence of masers in the surrounding area of candidates using the SIMBAD database and maser catalogs stored in VizieR. The idea of our search is to highlight those cluster candidates where maser emission is detected and then to provide a reference for the type of maser present. Table 2 lists the detected maser type, the source name (Col. 6), and a bibliographic reference for a catalog or discovery paper (Col. 7).

We have found that 128 cluster candidates are associated with maser emissions in a radius of 60″, with 50% of detections (63) within 10.5″ (Fig. 6). They correspond to 104 methanol masers, 72 water masers, and 55 hydroxyl masers. Detections of methanol and water masers are boosted by the efficiency of dedicated surveys carried out by Caswell et al. (2010), Caswell et al. (2011), and Green et al. (2012) for the methanol and Walsh et al. (2011) and Walsh et al. (2014) for water. It is interesting to note that 39 cluster candidates simultaneously include the detection of the three type of masers (methanol, hydroxyl, and water), putting particular emphasis on these cluster candidates. Breen et al. (2010) point out that the simultaneous detection of the three type of masers perhaps indicate a special moment in the evolution of newly formed stars; as these authors mention, the methanol masers are the first species to develop and also the first species to disappear, whereas both water and hydroxil masers are more persistent species.

YSOs are the primary tracers for star-forming regions. Catalogs of YSOs and YSO candidates in the area of Galactic disk covered by VVV survey include Mottram et al. (2007) and Yu & Wang (2014; derived from MSX data), Robitaille et al. (2008; derived from *Spitzer*/GLIMPSE data), and Chan et al. (1996; derived from IRAS data). Again, we performed a spatial cross-matching of star cluster candidates and YSO candidates extracted from the mentioned catalogs, using a 60″ radius. The procedure results in the detection of 207 YSOs candidates in the

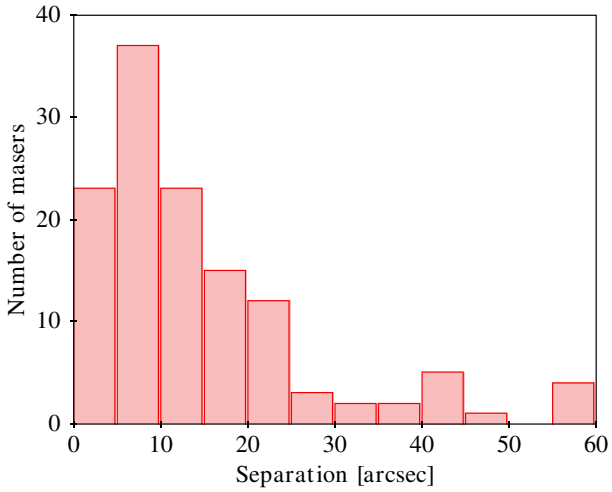

Fig. 6. Histogram of the number of masers associated with the new VVV–La Serena star cluster candidates.

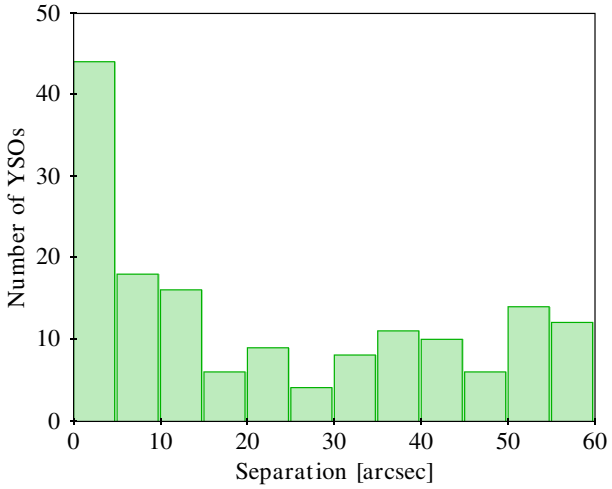

Fig. 7. Histogram of the number of YSO candidates associated with the new VVV–La Serena star cluster candidates.

area of 158 cluster candidates (32%), which are 50% of clusters with YSO candidates inside the 15″ circle, (Fig. 7).

Other interesting infrared tracers of ongoing star formation are outflows, EGOs (Cyganowski et al. 2008), and green fuzzies (Chambers et al. 2009). These last two types of objects have acquired their names from the remarkable 4.5 μm emission that is green in GLIMPSE color-composite images. EGOs and green fuzzies have been demostrated to be associated with young high-mass star forming regions (Chen et al. 2009, 2011). We searched for catalogs about outflows and outflows candidates in ViZieR, and found two additional catalogs. A search for ionized outflows toward high-mass YSO was carried out by Guzmán et al. (2012) through multifrequency radio continuum observations using the Australia Telescope Compact Array, and a catalog of molecular outflows recompiled by Wu et al. (2004). The cross-matching between La Serena cluster catalog with outflows and EGOs catalogs brings 73 clusters candidates associated with 90 outflows and EGO sources inside the circle with 60″ radius, where 50% are inside 6.2″ (see Fig. 8).

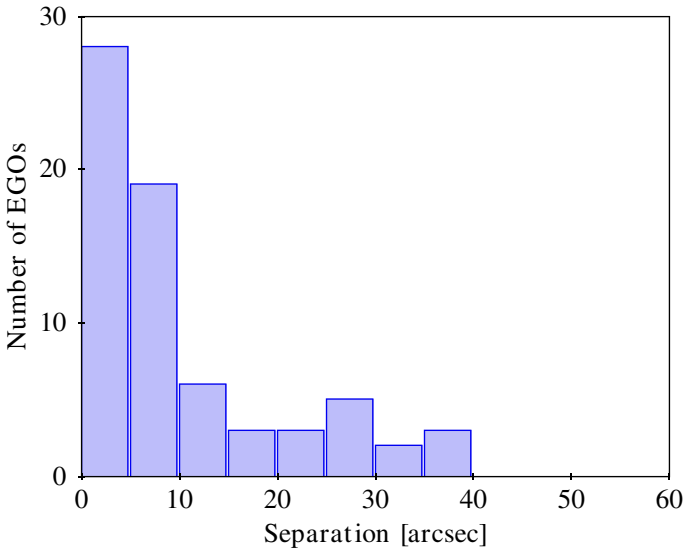

Fig. 8. Histogram of the number of EGO and outflow candidates associated with the new VVV–La Serena star cluster candidates.

5. Summary

We report the discovery of 493 new near-infrared stellar cluster candidates in a portion of the Galactic disk in the fourth quadrant using the ESO/Chile public survey VISTA Variables in the Vía Láctea. The analysis of the spatial distribution shows that the new clusters are concentrated near the Galactic plane and feature conspicuous local maxima, corresponding to large star-forming complexes, such as G305, RCW 95, RCW 106. Almost a half of the sample show a very compact appearance (250 candidates).

The majority of the discovered cluster candidates (456, 92%) are associated with dark infrared nebulosities, with 310 clusters directly associated to 552 cataloged dark clouds.

IRAS point sources are associated with 59% of cluster sample, while for the case of MSX point sources, the cross-matching gives 88% of the new cluster associated with a mid-infrared source. In view of the importance of identifying mid-infrared counterparts for the vast majority of new cluster candidates, we visually inspected GLIMPSE 8 μm images. The morphological richness of the images is noteworthy. In 292 cluster candidates show knotty morphology at 8 μm, 361 objects being associated with some kind of extended emission nebula at this wavelength regime. These morphologies suggest that most of the cluster candidates could be extremely young.

This scenario of extreme youth is reinforced by the cross-matching of the new cluster candidates against masers, YSO candidates, outflows, and EGOs. In the first instance, 128 clusters candidates have associated maser emission, with 104 of them methanol masers, which means excellent candidates for ongoing massive star formation. Special mention should be made of 39 cluster candidates that have three maser types associated: methanol, water and hydroxyl. For YSO candidates and outflows, 158 (32%) and 73 (15%) of new clusters candidates are closer than 60″ from them, respectively. In particular, there is a special set of sixteen cluster candidates that present a clear signpost of star-forming activity having associated simultaneosly dark nebulae, young stellar objects, extended green objects, and maser emission. The cluster candidates are La Serena numbers: 045, 115, 119, 161, 227, 228, 241, 283, 287, 316, 319, 391, 393, 410, 418, and 441.

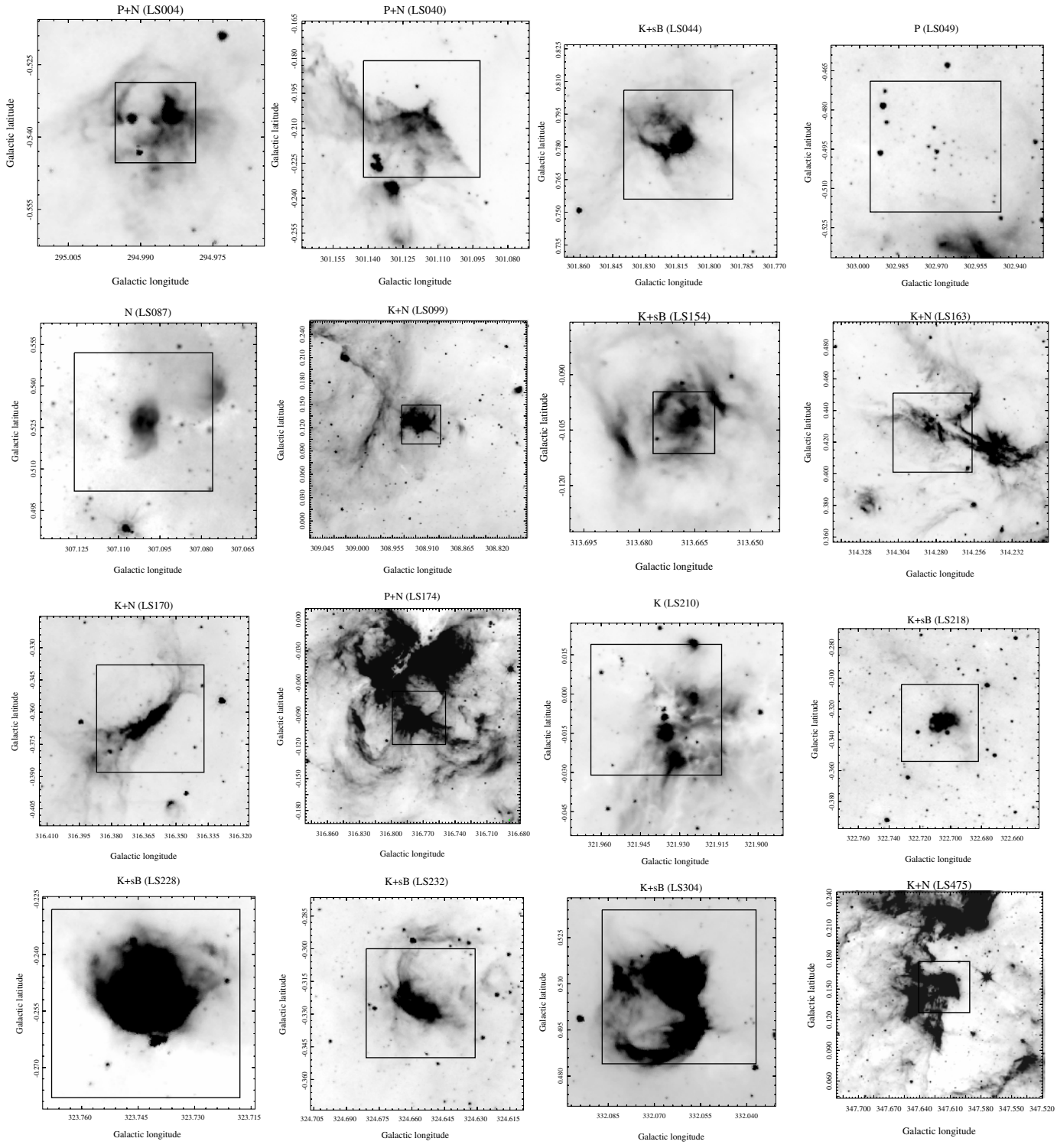

Fig. 9. Examples of different cluster morphologies based on images in the 8 μm band obtained with the Infrared Array Camera (IRAC) on board the *Spizer* Space Telescope. Boxes inside each panel correspond to the cluster candidate charts shown in Fig. 1.

Again, these findings suggest that a substantial proportion of the discovered clusters are very young and have ongoing star formation. This scenario is consistent with the common features of the majority of the clusters discovered independently by Borissova et al. (2011) and Solin et al. (2014), using the same VVV DR1 images.

Up to now, the vast majority of star cluster candidates discovered on the basis of VVV images are quite compact and generally surrounded by bright or dark nebulosities. With this work, we think that we are getting a deeper level of discovery using the VVV survey in the Galactic disk. But much remains to explore in relation to the population of slightly evolved young clusters, where the detectable low-mass stars have left the accretion phase. After this phase, the clusters have dissipated much of the molecular cloud in which they formed, and some of the most massive and notable members have evolved or have been ejected and may show a lower concentration. These clusters are very difficult to separate the contaminating population of the disk of the galaxy. A further opportunity to squeeze information from the VVV survey is to exploit the stack of K_S-band

images obtained during the current synoptic stage of the project. At present, VVV is gathering dozens of K_S-band images that can be the raw material for pursuiting further immersed and fainter stellar clusters.

Note added in proof. After this paper was submitted, we became aware of a paper by Morales et al. (2013) which list 695 clusters within the Galactic range $|l| \leq 60^\circ$ and $|b| \leq 1.5^\circ$ covered by the ATLASGAL survey, which was used to search for correlations with submm dust continuum emission tracing dense molecular gas. From that list, 393 clusters are in the area covered by the VVV Galactic disk observations. The cross-matching procedure between Morales et al. (2013) catalog and our list using a matching radius of 60 arcsec results in 31 clusters (6.3%) in common.

Acknowledgements. We thank the anonymous referee for the very useful suggestions that helped us improve this work. R.H.B. acknowledges support by FONDECYT Regular project No. 1120668. A.R.L. is grateful for financial support from ALMA-CONICYT Fund, and Dirección de Investigación of Universidad de La Serena through project DIULS REGULAR PR13144. J.L.N.C. also acknowledges financial support from the ALMA-CONICYT postdoctoral program No. 31120026. M.S. acknowledges support from ESO-Chile Joint Committee and "Becas Chile de Postdoctorado en el Extranjero" project No. 74150088. V.F. acknowledges support from the ESO-Chile Joint Committee and DIULS. M.H. acknowledges the support of the Basal PFB-06 and the Milenio Milky Way Nucleus. We gratefully acknowledge use of data from the ESO Public Survey programme ID 179.B-2002, taken with the VISTA telescope, data products from the Cambridge Astronomical Survey Unit, and funding from the FONDAP Center for Astrophysics 15010003, the BASAL CATA Center for Astrophysics and Associated Technologies PFB-06, and the Millennium Institute of Astrophysics MAS. D.M. acknowledge financial support from CONICYT by Proyecto FONDECYT Regular No. 1130196. R.K.S. acknowledges support from CNPq/Brazil through projects 310636/2013-2 and 481468/2013-7. This research has made use of SIMBAD, VizieR, and "Aladin sky atlas" operated and developed at CDS, Strasbourg Observatory, France. Also, this research has made use of NASA's Astrophysics Data System.

References

Beichman, C. A., Neugebauer, G., Habing, H. J., Clegg, P. E., & Chester, T. J. 1988, Infrared Astronomical Satellite (IRAS) catalogs and atlases, Vol. 1: Explanatory supplement, 1
Benaglia, P., Ribó, M., Combi, J. A., et al. 2010, A&A, 523, A62
Benjamin, R. A., Churchwell, E., Babler, B. L., et al. 2003, PASP, 115, 953
Bica, E., Dutra, C., Soares, J., & Barbuy, B. 2003, A&A, 404, 223
Bonatto, C., Kerber, L. O., Bica, E., & Santiago, B. X. 2006, A&A, 446, 121
Bonnarel, F., Fernique, P., Bienayme, O., et al. 2000, A&AS, 143, 33
Borissova, J., Bonatto, C., Kurtev, R., et al. 2011, A&A, 532, A131
Breen, S. L., Caswell, J. L., Ellingsen, S. P., & Phillips, C. J. 2010, MNRAS, 406, 1487
Breen, S. L., Ellingsen, S. P., Contreras, Y., et al. 2013, MNRAS, 435, 524
Carpenter, J. M., Snell, R. L., & Schloerb, F. P. 1995, ApJ, 450, 201
Carpenter, J. M., Heyer, M. H., & Snell, R. L. 2000, ApJS, 130, 381
Caswell, J. L., Fuller, G. A., Green, J. A., et al. 2010, MNRAS, 404, 1029
Caswell, J. L., Fuller, G. A., Green, J. A., et al. 2011, MNRAS, 417, 1964
Chambers, E. T., Jackson, J. M., Rathborne, J. M., & Simon, R. 2009, ApJS, 181, 360
Chan, S. J., Henning, T., & Schreyer, K. 1996, A&AS, 285
Chen, X., Ellingsen, S. P., & Shen, Z.-Q. 2009, MNRAS, 396, 1603
Chen, X., Ellingsen, S. P., Shen, Z.-Q., Titmarsh, A., & Gan, C.-G. 2011, ApJS, 196, 9
Churchwell, E., Povich, M. S., Allen, D., et al. 2006, ApJ, 649, 759
Clark, J. S., Negueruela, I., Davies, B., et al. 2009, A&A, 498, 109
Cyganowski, C. J., Whitney, B. A., Holden, E., et al. 2008, AJ, 136, 2391
Dalton, G. B., Caldwell, M., Ward, A. K., et al. 2006, Proc. SPIE, 6269, 30
de Zeeuw, P. T., Hoogerwerf, R., de Bruijne, J. H. J., Brown, A. G. A., & Blaauw, A. 1999, AJ, 117, 354
Dobashi, K. 2011, PASJ, 63, S1
Dutra, C. M., & Bica, E. 2002, A&A, 383, 631
Dutra, C. M., Bica, E., Soares, J., & Barbuy, B. 2003, A&A, 400, 533
Egan, M. P., Price, S. D., Kraemer, K. E., et al. 2003, VizieR Online Data Catalog: V/114
Ellignsen, S. P. 2006, ApJ, 638, 241
Emerson, J., & Sutherland, W. 2010, The Messenger, 139, 2
Figer, D. F., MacKenty, J. W., Robberto, M., et al. 2006, ApJ, 643, 1166
Froebrich, D., Scholz, A., & Raftery, C. L. 2007, MNRAS, 374, 399
Green, J. A., Caswell, J. L., Fuller, G. A., et al. 2012, MNRAS, 420, 3108
Guzmán, A. E., Garay, G., Brooks, K. J. & Voronkov, M. A. 2012, ApJ, 753, 51
Hartley, M., Tritton, S. B., Manchester, R. N., Smith, R. M., & Goss, W. M. 1986, A&AS, 63, 27
Karampelas, A., Dapergolas, A., Kontizas, E., et al. 2009, A&A, 497, 703
Kirsanova, M. S., Sobolev, A. M., Thomasson, M., et al. 2008, MNRAS, 388, 729
Kumar, M. S. N., Kamath, U. S., & Davies, C. J. 2004, MNRAS, 353, 1025
Kumar, M. S. N., Keto, E., & Clerkin, E. 2006, A&A, 449, 1033
Lada, E. A., & Lada, C. J. 1995, AJ, 109, 1682
Lada, C. J., & Lada, E. A. 2003, ARA&A, 41, 57
López, C., Bronfman, L., Nyman, L.-Å, May, J., & Garay, G. 2011, A&A, 534, A131
Lucas, P. W., Hoare, M. G., Longmore, A., et al. 2008, MNRAS, 391, 136
Mercer, E. P., Clemens, D. P., Meade, M. R., et al. 2005, ApJ, 635, 560
Mottram, J. C., Hoare, M. G., Lumsden, S. L., et al. 2007, A&A, 476, 1019
Maciejewski, G., & Niedzielski, A. 2008, Astron. Nachr., 329, 602
Morales, E. F. E., Wyrowski, F., Schuller, F., & Menten, K. M. 2013, A&A, 560, A76
Minniti, D., Lucas, P. W., Emerson, J. P., et al. 2010, New Astron., 15, 433
Moni Bidin, C., de La Fuente Marcos, R., de La Fuente Marcos, C., & Carraro, G. 2010, A&A, 510, A44
Odenkirchen, M., & Soubiran, C. 2002, A&A, 383, 163
Peretto, N., & Fuller, G. A. 2009, A&A, 505, 405
Portegies Zwart, S. F., McMillan, S. L. W., & Gieles, M. 2010, ARA&A, 48, 431
Robitaille, T. P., Meade, M. R., Babler, B. L., et al. 2008, AJ, 136, 2413
Saito, R. K., Hempel, M., Minniti, D., et al. 2012, A&A, 537, A107
Skrutskie, M. F., Cutri, R. M., Stiening, R., et al. 2006, AJ, 131, 1163
Solin, O., Haikala, L., & Ukkonen, E. 2014, A&A, 562, A115
Taylor, M. B. 2005, Astronomical Data Analysis Software and Systems XIV, 347, 29
Tian, K. P., van Leeuwen, F., Zhao, J. L., & Su, C. G. 1996, A&AS, 118, 503
Walsh, A. J., Breen, S. L., Britton, T., et al. 2011, MNRAS, 416, 1764
Walsh, A. J., Purcell, C. R., Longmore, S. N., et al. 2014, MNRAS, 442, 2240
Wu, Y., Wei, Y., Zhao, M., et al. 2004, A&A, 426, 503
Yu, N., & Wang, J.-J. 2014, MNRAS, 440, 1213